
Check for updates

technique of picosecond Laser-induced abla… spectrometry (LIA-QMS) [16]. It is one of a limited num… mortem analysis diagnostics which allows quantitative and depth-re… solved information of the hydrogen content in graphite components. As a residual gas analysis, only volatile sample components can be detected, which is why LIBS is performed simultaneously in one setup. Compared to LID-QMS, the ablation process in the presented picosecond LIA-QMS method gives depth-resolved information and the plasma formation enables spectroscopic measurements.

This contribution consists of five sections: The introduction is followed by information concerning samples from W7-X and plasma exposure conditions (Section 2). The combined setup for LIBS and LIA-QMS as well as details to these techniques are presented in Section 3. Limiter tile analysis results comparing three different limiters in poloidal and toroidal direction and a discussion are shown in Section 4. Finally, a conclusion is given in Section 5.

2. Samples

In operation phase 1.1, five equivalent graphite limiters were installed in W7-X [13]. They were exposed to helium and hydrogen plasmas with a total exposure time of about 311 s [17]. Each limiter consists of nine tiles. The analyzed positions with their labels are shown in Fig. 1. The overlay shows a simulation of EMC3-EIRENE code [18] for the heat flux in a standard magnetic configuration of W7-X hydrogen plasma. Two stripes of high heat fluxes in poloidal direction are observed on the limiter. Their maxima are detected on tiles 3 and 6 for the left and right side of the limiter respectively. The simulation predicts an asymmetry in toroidal direction of one limiter tile due to the imposed magnetic field structure with different connection lengths [13]. Moreover, an asymmetry on one limiter in poloidal direction is predicted.

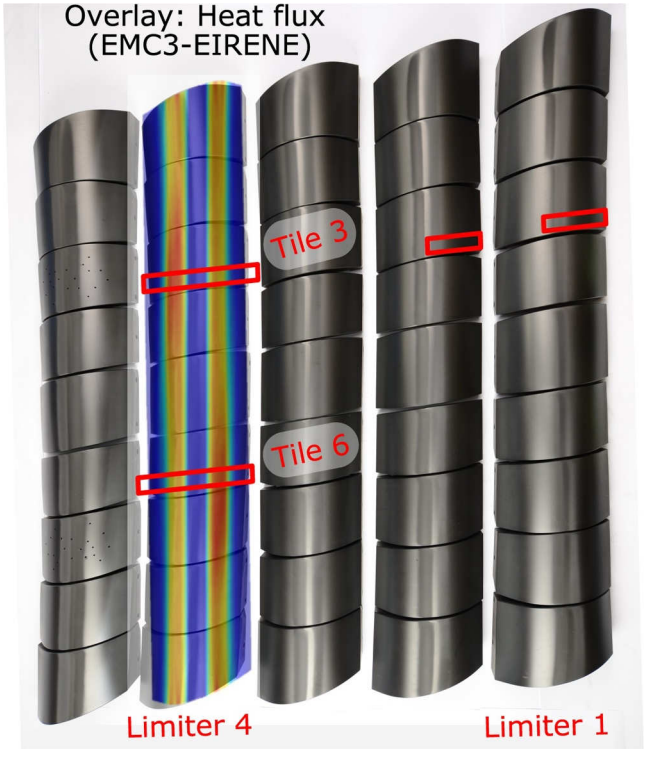

Fig. 1. Photo of limiter modules 5 to 1 (left to right), each containing nine tiles. Analyzed tiles are marked in red. On limiter 4 a simulation of the heat flux (EMC3-EIRENE code [13]) owing to electron and ion impact is overlayed. (For interpretation of the references to colour in this figure legend, the reader is referred to the web version of this article.)

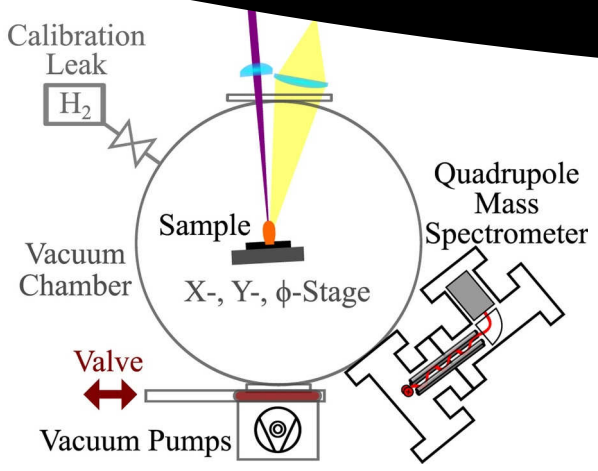

Fig. 2. Schematic overview of the setup: Single picosecond laser pulses are used to successive ablate a sample in a vacuum chamber. A combination of LIBS and QMS is used to measure the sample's composition. For a residual gas analysis and the calibration of the quadrupole mass spectrometer a valve to the vacuum pumps is closed (figure based on [16]).

Here, we use the hydrogen content in the tiles to study if the asymmetries in the impinging ion and heat flux can be observed by post-mortem analysis techniques. Additionally, a comparison of limiter 1, 2 and 4 is shown, as limiter 1 was positioned slightly deeper into the plasma and received higher heat loads [13].

3. Experimental setup

The experimental setup for picosecond laser-induced ablation using a Nd:YVO_4 laser by *EKSPLA* is shown in Fig. 2. The samples are mounted on a *x*-, *y*-, ϕ-stage in a vacuum chamber with a base pressure of $p_0 = 1 \times 10^{-7}$ mbar. The limiter tiles are cut into 7 pieces to reduce a change of the laser fluence caused by its curved surface. This results in an angle between the laser pulses and the samples surface of $90^\circ \pm 5^\circ$. An increase of the laser spot size is neglected. To perform residual gas analysis after single shot laser-induced ablation (LIA-QMS), a valve to the vacuum pumps can be closed. Simultaneously, LIBS is performed with an observation angle of 85°. The focal lengths of the biconvex collimation lens and the planoconvex focusing lens are $f = 100$ mm and $f = 500$ mm respectively. Applied laser parameter and settings are shown in Table 1.

3.1. Diagnostics

With the setup shown in Fig. 2, LIA-QMS and LIBS are performed simultaneously to get sample composition information from characteristic line radiation (LIBS) with additional quantitative information

Table 1
Overview of the laser parameter and settings used for the single shot analysis of W7-X graphite limiter tiles.

Laser wavelength:	λ_L	= 355 nm
Pulse duration:	t_L	= 35 ps
Pulse energy:	E_L	= 25 mJ
Spot diameter at sample:	d_L	= 700 µm
Average laser fluence:	F_L	= 6.5 $\frac{J}{cm^2}$

of volatile species (LIA-QMS). Using the laser [illegible] Table 1, a depth resolution of ≈ 100 nm and a lateral resolution to 2 mm is achieved.

In addition, TDS was performed with pieces ($l \times w \times h = (8 \times 8 \times 4)\text{mm}^3$) of the limiter tiles, assuming there was no modification of the composition for material deeper than 4 mm due to plasma operation in W7-X. TDS is used as independent measure of the quantitative hydrogen content, without any depth resolution, but as integral measure.

3.1.1. LIA-QMS

Laser-induced ablation-quadrupole mass spectrometry is a relatively novel method to measure volatile sample components. After closing a valve to the vacuum pumps, a high energetic picosecond laser pulse is focused on the sample surface. The partial pressure of removed material in gas phase with $\frac{m}{z}$ up to $100\frac{\text{amu}}{\text{e}}$ is detected in quasi-equilibrium[1] with a quadrupole mass spectrometer. Details on the measurement technique can be found in [16]. After 15 subsequent laser pulses on one sample position of the limiter tiles, a constant measurement signal is observed. For all LIA-QMS data shown in this publication, this constant signal is subtracted as background. Consequently, only the composition modifications, caused by exposure to W7-X plasma, close to the surface are analyzed, whereas intrinsic components and parasitic signals from interaction of the laser radiation with the chamber wall are subtracted. The measurement signals can be quantified by TDS results (Table 2) or by using a calibration leak (described in [16]).

3.1.2. LIBS

For laser-induced breakdown spectroscopy a single-core fiber with a diameter of 600 µm and a numerical aperture of 0.22 transports emitted light into a Ocean Optics, *HR2000* USB spectrometer. The wavelength range is 350 nm to 800 nm with spectral resolution of about 1 nm (FWHM). More details on the LIBS setup and its applications for analysis of the limiter tiles can be found in [15]. LIBS data uses hydrogen and carbon peak intensities for a qualitative comparison with LIA-QMS results.

4. Results and discussion

The surface composition of different positions on the graphite limiters is analyzed. Fig. 3 shows a photo of limiter 4 - tile 3 with labeling for toroidal and poloidal scanning direction.

4.1. Local distribution of hydrogen on limiter 4

A scan over the limiter tiles in toroidal direction with a lateral resolution up to 2 mm is performed. The integrated signal of ten successive laser-induced ablations, giving a total ablation depth of 1 µm is shown in Fig. 4 for tile 3 and 6. Regarding tile 3, the hydrogen content shows a symmetry for the left and right part with two maxima on each side of the limiter. The maximum at the outside of the right side ($x \approx 70$ mm) of the tile is slightly broader than the on the left side, which is attributed to the shape of the limiter.

Fig. 5 shows the depth resolved LIA-QMS hydrogen signals for the local extremes of tile 3 in Fig. 4. Fig. 6 shows LIBS results at the same positions. The laser-induced ablation rate for the top x-axis was measured ex-situ with a profilometer and approximated to be equivalent for the different layer structures. The depth distribution of the hydrogen content is different in these four zones on the limiter, which is consistent with microscopy measurements in these regions [14]:

[1] The term *quasi-equilibrium* is used to describe a constant partial pressure, caused by laser-induced sample ablation, which is superposed with a linear rise of the background signal, caused by outgassing of the vacuum chamber wall.

Sample	[illegible] (10^{18} H atoms)	[illegible]
Reference	(0.80 ± 0.12)	-
Mixed	(1.79 ± 0.27)	(1.55 ± 0.60)
Net-erosion	(1.04 ± 0.16)	(0.38 ± 0.43)
Net-deposition	(2.00 ± 0.30)	(1.88 ± 0.66)

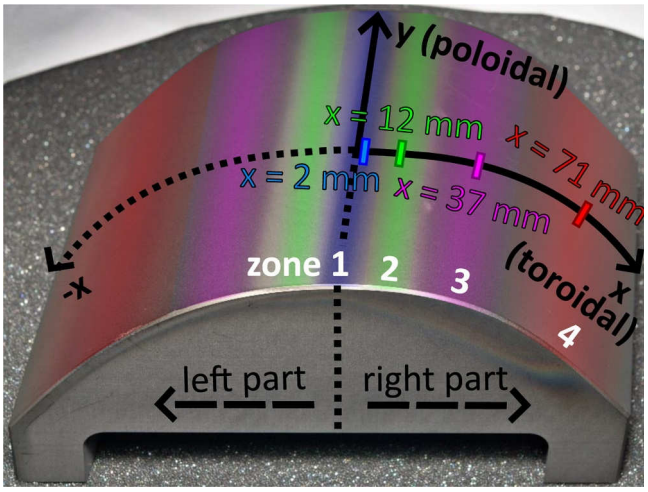

Fig. 3. Photo of limiter 4 - tile 3 with lateral position x in toroidal direction. The colored regions show the identified zones (figure based on [15]).

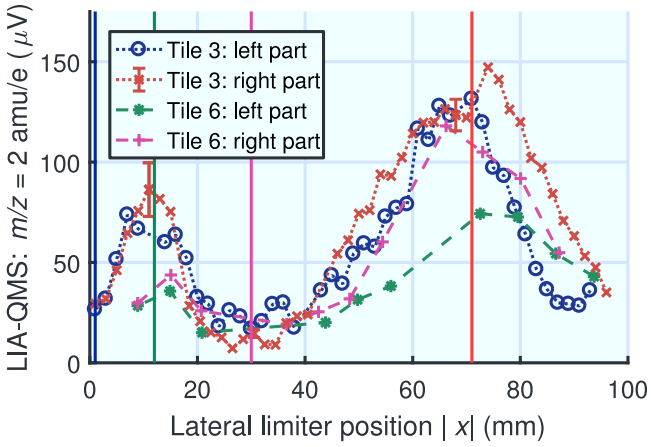

Fig. 4. LIA-QMS hydrogen signals of limiter 4 - tiles 3 and 6 over toroidal direction x as surface coordinate with 0 at the center of the limiter. The signals are folded to show the symmetry for the left and right side of the limiters. The vertical lines show the centers of the identified zones.

- In the limiter center (x = 0 mm)-almost tangential to the plasma a low hydrogen content is observed. This plasma-wetted zone is erosion-dominated due to high surface temperature and energy of incident particles.
- Near the limiter center (x = (12 ± 5) mm) a mixed zone with high hydrogen content in small depth is observed. Local redeposition partially coats the surface of the limiter in this section [14], causing a higher hydrogen content than in the limiter center for LIA-QMS and LIBS analysis.
- Next to this area (x = (30 ± 10) mm) a small amount of hydrogen indicates a pure erosion zone where hydrogen is only implanted in

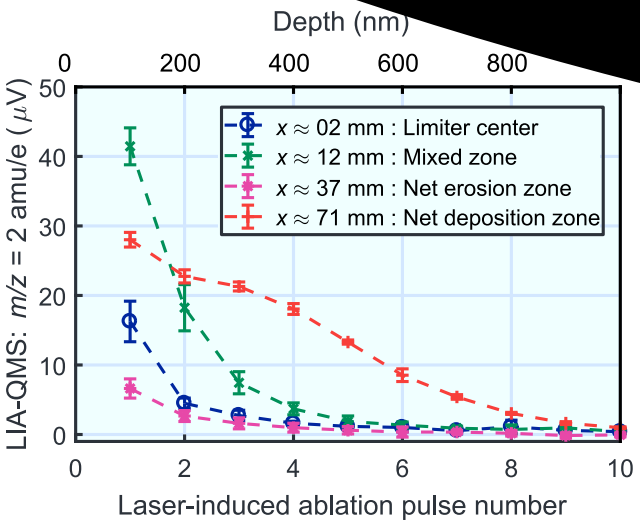

Fig. 5. Depth resolved LIA-QMS hydrogen signal for different toroidal positions x on limiter 4 - tile 3 which show zones of different plasma interaction with the surface.

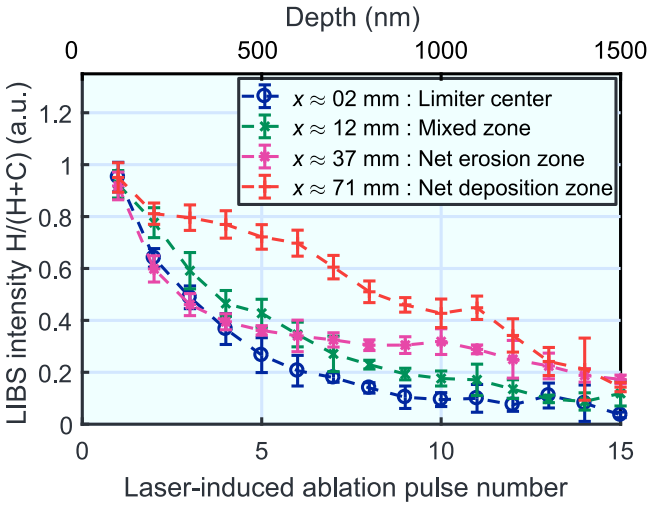

Fig. 6. Depth resolved LIBS signal on limiter 4 - tile 3.

the material.

- On the outer part of the limiter tile (x = (70 ± 20) mm), located deepest in the scrape-off layer, a net-deposition zone is observed: A layer of re-deposited carbon and co-deposited hydrogen with a thickness up to 600 μm is formed during OP 1.1. The thickness is in good agreement with EDX measurements [15].

The depth resolved LIA-QMS and LIBS signals both show the highest hydrogen content in the net deposition zone from laser-induced ablation pulse number 2–9. Moreover, in the mixed zone the second highest signals are measured for pulse number 2–5. For the pulse numbers 5–10 in the net erosion zone the implanted hydrogen can only be detected with LIBS. The overall erosion/deposition pattern with an erosion dominated center part and strong deposition on the side areas is comparable to observation in limiter tokamaks [3,19].

4.2. Poloidal distribution of hydrogen

Comparable hydrogen contents and depth distributions are found for the net-deposition zone of the right part of tile 3 and tile 6 (Fig. 4), although an asymmetry of the heat flux on the limiter tiles is observed (compare Fig. 1 and [14]).

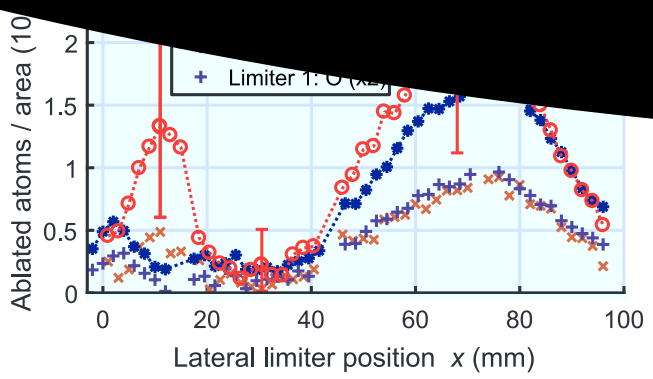

Fig. 7. Comparison of the hydrogen and oxygen content of limiter tiles 3 measured with LIA-QMS in different modules of W7-X.

For tile 6, the left part shows a 30% lower hydrogen signal in the net-deposition zone. Also the hydrogen content of tile 6 in the mixed zone is 50% lower than on tile 3.

4.3. Global distribution of hydrogen and oxygen in toroidal direction

Fig. 7 shows a comparison of limiter 1 and limiter 4 - tile 3 in toroidal direction. Within the measurement uncertainty, limiter 1 shows a similar amount of hydrogen and oxygen in the net-deposition zone, whereas the signals of limiter 1 in the mixed zone are small compared to the erosion dominated zone. This is attributed to the fact, that limiter 1 was exposed to up to 2 times higher heat load [13] associated with significant higher surface temperature which causes less hydrogen stored in the layer.

The difference in hydrogen content between limiters 2 and 4 is within 0.2×10^{22} atoms/m^2 (not shown), and thus below the measurement uncertainty.

The signals in Fig. 7 were calibrated using TDS results of the deposition zone on limiter 4, which is discussed in more detail in Section 4.4.

4.4. Quantification

To quantify the LIA-QMS results, two calibration procedures can be used: On the one hand, TDS measurements using small pieces of the limiter tiles was performed. On the other hand a calibration leak, which is integrated in the setup, can be used with each analyzed gas. TDS results are shown in Table 2.

To minimize measurement uncertainties, all pieces were cut to the same dimensions. A graphite limiter tile which was not installed in W7-X (*Reference sample*) was outgassed to determine the hydrogen content in the graphite before plasma exposure. After subtraction of the reference's hydrogen content, the signals of pieces from the center of the identified zones were normalized to the exposed surface area. This evaluation extracts the plasma-induced hydrogen signal.[2] In the net-erosion zone, hydrogen can only be implanted, resulting in a low hydrogen TDS signal as well as LIA-QMS signal for $\frac{m}{z} = 2\frac{\text{amu}}{\text{e}}$. For the mixed and net-deposition zone, additionally a layer of re-deposited carbon with co-deposited hydrogen and oxygen [14] results in a 4 to 5 times higher hydrogen signal. Moreover, the TDS results show 10% lower hydrogen content in the mixed zone compared to the deposition

[2] For error calculations the uncertainty of the calibration leak of 10% is used for TDS. The sample size uncertenties are Δx_i = 0.1 mm. Hydrogen contamination from the sides of the samples after cutting is neglected.

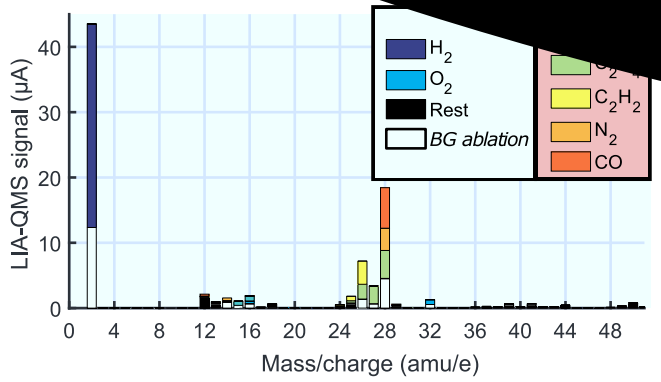

Fig. 8. Possible solution for the composition analysis of the first laser pulse in the deposition dominated zone. Pulse number 15 in white is showing the constant background (*BG ablation*) signal. (For interpretation of the references to colour in this figure legend, the reader is referred to the web version of this article.)

zone, whereas the signal is about 50% lower for LIA-QMS (Fig. 4) and LIBS [15].

Using TDS as calibration for LIA-QMS requires an additional post-mortem analysis procedure with lower lateral resolution and without depth information. Another method to quantify the quadrupole signal bases on a calibration leak with known flow rate: With closed shutter to the vacuum pumps, hydrogen gas is filled into the vacuum chamber with a flow rate of $\Delta Q H_2 = (9.13 \pm 0.73) \times 10^{-7}$Pa m^3/s. Using the quadrupole detector current rise and the flow rate, the detector signal can be converted to a hydrogen partial pressure and hence to an absolute number of hydrogen atoms when the ideal gas equation is applied. Details to this calibration procedure can be found in [16]. With this calibration method, the hydrogen content is 35% lower than for TDS in the mixed and the net-deposition zone. Potential reasons for the discrepancy are the following. Firstly, hydrogen can be implanted deeper in the material than 1 μm, so that is not detected by LIA-QMS, but outgassed with TDS. Also the unexposed reference sample might be slightly different in its hydrogen content. Moreover, for picosecond laser-induced ablation, the induced plasma does not necessarily break all chemical bonds during the ablation process. Consequently, a fraction of the hydrogen remains in hydrocarbons. A composition analysis is performed by sweeping the quadrupole for $\frac{m}{z} = 2\frac{\text{amu}}{\text{e}} - 100\frac{\text{amu}}{\text{e}}$ to show the ablated hydrocarbons.

4.5. Surface composition analysis with LIA-QMS

A residual gas spectrum for the first laser-induced ablation pulse on limiter 4 - tile 3 in the net-deposition zone is shown in Fig. 8. The constant laser-induced signal after 15 laser pulses is overlayed as background signal (*BG ablation*) in white. Besides hydrogen ($\frac{m}{z} = 2\frac{\text{amu}}{\text{e}}$) and oxygen ($\frac{m}{z} = (32 \text{ and } 16)\frac{\text{amu}}{\text{e}}$), LIA-QMS analysis shows significant signals for (12–16) $\frac{\text{amu}}{\text{e}}$ and (25–28) $\frac{\text{amu}}{\text{e}}$. A possible solution for the composition analysis with hydrocarbons, nitrogen and carbon monoxide is presented.[3]

The C_2H_x signals for $\frac{m}{z} = (25 - 27)\frac{\text{amu}}{\text{e}}$ indicate, that after picosecond laser-induced ablation of the net-deposition layer, carbon hydrides needs to be included for quantitative analysis using LIA-QMS. The signal of $\frac{m}{z} = 28\frac{\text{amu}}{\text{e}}$ is a superposition of hydrocarbons, nitrogen and carbon monoxide. As the signal of $\frac{m}{z} = 30\frac{\text{amu}}{\text{e}}$ is low, no significant amount of C_2H_6 seems to be ablated. A drawback of quantitative LIA-

[3] Cracking patterns for O_2, N_2 and CH_4 were measured using gas inlet by the calibration leak. As the results are in good agreement ($\Delta I < 5\%$) with mass spectra from Linstrom and Mallard [20], its cracking patterns were included for C_2H_2 and C_2H_4 in Fig. 8.

5. Conclusion

LIA-QMS results for the hydrogen content of graphite from W7-X OP 1.1 are in good agreement with LIBS measurements. In toroidal direction LIA-QMS analysis shows, that signals of hydrogen and oxygen close to the limiter center are lower for limiter 1 than for limiter 2 and 4. This implies that no mixed zone is present on limiter 1 as the erosion rate is higher than the deposition rate near the limiter center, caused by a two times higher heat flux on this limiter tile. In poloidal direction, no significant variation of the hydrogen content is observed for the deposition dominated zone, whereas the hydrogen content in the mixed zone of tile 6 is 50% lower than in the mixed zone of tile 3.

A composition analysis of the residual gas spectrum shows, that hydrocarbons include a significant fraction of the total amount of hydrogen in the sample. These need to be included for quantitative hydrogen content measurements using LIA-QMS analysis and also to be considered for the interpretation of picosecond LIBS results.

Future analysis will be performed with graphite divertor tiles from OP 1.2. Furthermore, LIA-QMS technique will be improved and tested as a possible in-situ diagnostic for hydrogen retention monitoring in fusion devices.

Acknowledgment

This work has been carried out within the framework of the EUROfusion Consortium and has received funding from the Euratom research and training programme 2014–2018 under grant agreement No 633053. The views and opinions expressed herein do not necessarily reflect those of the European Commission.

Supplementary material

Supplementary material associated with this article can be found, in the online version, at 10.1016/j.nme.2018.12.019.

References

[1] S. Brezinsek, M. Jakubowski, Plasma-surface interaction and plasma-edge studies in Wendelstein 7-X operating with passively cooled graphite divertor, 45th EPS Conference on Plasma Physics, I3.111, (2018).
[2] O. Neubauer, W. Biel, G. Czymek, P. Denner, F. Effenberg, A. Krämer-Flecken, Y. Liang, O. Marchuk, G. Offermanns, M. Rack, U. Samm, O. Schmitz, B. Schweer, A. Terra, Diagnostic setup for investigation of plasma wall interactions at Wendelstein 7-X, Fusion Eng. Des. 96–97 (2015) 891–894, https://doi.org/10.1016/j.fusengdes.2015.06.102.
[3] A. Kirschner, V. Philipps, J. Winter, Simulation of the plasma - wall interaction in a tokamak with the Monte Carlo code ERO-TEXTOR, Nucl. Fusion 40 (5) (2000) 989, https://doi.org/10.1088/0029-5515/40/5/311.
[4] T.S. Pedersen, M. Otte, et al., Confirmation of the topology of the Wendelstein 7-X magnetic field to better than 1:100,000, Nat. Commun. 7 (December) (2016), https://doi.org/10.1038/ncomms13493.
[5] T.S. Pedersen, A. Dinklage, Y. Turkin, R. Wolf, S. Bozhenkov, J. Geiger, G. Fuchert, H.S. Bosch, K. Rahbarnia, H. Thomsen, U. Neuner, T. Klinger, A. Langenberg, H. Trimiño Mora, P. Kornejew, J. Knauer, M. Hirsch, N. Pablant, Key results from the first plasma operation phase and outlook for future performance in Wendelstein 7-X, Phys. Plasmas 24 (5) (2017) 0–10, https://doi.org/10.1063/1.4983629.
[6] J. Roth, E. Tsitrone, A. Loarte, T. Loarer, G. Counsell, R. Neu, V. Philipps, S. Brezinsek, M. Lehnen, P. Coad, C. Grisolia, K. Schmid, K. Krieger, A. Kallenbach, B. Lipschultz, R. Doerner, R. Causey, V. Alimov, W. Shu, O. Ogorodnikova, A. Kirschner, G. Federici, A. Kukushkin, Recent analysis of key plasma wall interactions issues for ITER, J. Nucl. Mater. 390–391 (1) (2009) 1–9, https://doi.org/10.1016/j.jnucmat.2009.01.037.
[7] V. Philipps, A. Malaquias, A. Hakola, J. Karhunen, G. Maddaluno, S. Almaviva, L. Caneve, F. Colao, E. Fortuna, P. Gasior, M. Kubkowska, A. Czarnecka, M. Laan, A. Lissovski, P. Paris, H.J. van der Meiden, P. Petersson, M. Rubel, A. Huber, M. Zlobinski, B. Schweer, N. Gierse, Q. Xiao, G. Sergienko, Development of laser-based techniques for in situ characterization of the first wall in ITER and future fusion devices, Nucl. Fusion 53 (9) (2013) 93002, https://doi.org/10.1088/0029-

5515/53/9/093002.
[8] A. Malaquias, V. Philipps, A. Huber, A. Hakola, J. Likonen, J. K…
S. Tervakangas, M. Aints, P. Paris, M. Laan, A. Lissovski, S. Almaviva, L. …
F. Colao, G. Maddaluno, M. Kubkowska, P. Gasior, H.J.V.D. Meiden, A.R. Lof, P.A.Z.V. Emmichoven, P. Petersson, M. Rubel, E. Fortuna, Q. Xiao, Development of ITER relevant laser techniques for deposited layer characterisation and tritium inventory, J. Nucl. Mater. 438 (2013) S936–S939, https://doi.org/10.1016/j.jnucmat.2013.01.203.
[9] D.W. Hahn, N. Omenetto, Laser-induced breakdown spectroscopy (LIBS), part II: review of instrumental and methodological approaches to material analysis and applications to different fields, Appl. Spectrosc. 66 (4) (2012) 347–419, https://doi.org/10.1366/11-06574.
[10] R. Fantoni, S. Almaviva, L. Caneve, F. Colao, A.M. Popov, G. Maddaluno, Development of calibration-Free laser-Induced-Breakdown-Spectroscopy based techniques for deposited layers diagnostics on ITER-like tiles, Spectrochim. Acta - Part B At. Spectrosc. 87 (2013) 153–160, https://doi.org/10.1016/j.sab.2013.05.032.
[11] M. Zlobinski, Laser Induced Desorption as Hydrogen Retention Diagnostic Method, Berichte des Forschungszentrums Jülich, 2016 Ph.D. thesis. 4396
[12] G. De Temmerman, M.J. Baldwin, D. Anthoine, K. Heinola, A. Jan, I. Jepu, J. Likonen, C.P. Lungu, C. Porosnicu, R.A. Pitts, Efficiency of thermal outgassing for tritium retention measurement and removal in ITER, Nucl. Mater. Energy 12 (2017) 267–272, https://doi.org/10.1016/j.nme.2016.10.016.
[13] G.A. Wurden, C. Biedermann, F. Effenberg, M. Jakubowski, H. Niemann, L. Stephey, S. Bozhenkov, S. Brezinsek, J. Fellinger, B. Cannas, F. Pisano, S. Marsen, H.P. Laqua, R. König, O. Schmitz, J.H. Harris, E.A. Unterberg, Limiter observations during W7-X first plasmas, Nucl. Fusion 57 (056036) (2017), https://doi.org/10.1088/1741-4326/aa6609.
[15] C. Li, N. Gierse, …
T.S. Pedersen, R. König, Y. …
spectroscopy for Wendelstein 7-X stellarator …
(2017), https://doi.org/10.1088/0031-8949/2017/T170/014004.
[16] J. Oelmann, N. Gierse, C. Li, S. Brezinsek, M. Zlobinski, B. Turan, S. Haas, C. Linsmeier, Depth-resolved sample composition analysis using laser-induced ablation-quadrupole mass spectrometry and laser-induced breakdown spectroscopy, Spectrochim. Acta - Part B At. Spectrosc. 144 (2018) 38–45, https://doi.org/10.1016/j.sab.2018.03.009.
[17] R.C. Wolf, A. Ali, et al., Major results from the first plasma campaign of the Wendelstein 7-X stellarator, Nucl. Fusion 57 (10) (2017) 102020, https://doi.org/10.1088/1741-4326/aa770d.
[18] Y. Feng, J. Kisslinger, Status and application of the EMC3 / EIRENE code, Contrib. Plasma Phys. 40 (3–4) (2000) 271–275, https://doi.org/10.1002/1521-3986(200006)40:3/4<271::AID-CTPP271>3.0.CO;2-1.
[19] S. Brezinsek, A. Pospieszczyk, D. Borodin, M.F. Stamp, R. Pugno, A.G. McLean, U. Fantz, A. Manhard, A. Kallenbach, N.H. Brooks, M. Groth, P. Mertens, V. Philipps, U. Samm, Hydrocarbon injection for quantification of chemical erosion yields in tokamaks, J. Nucl. Mater. 363–365 (1–3) (2007) 1119–1128, https://doi.org/10.1016/j.jnucmat.2007.01.190.
[20] P.J. Linstrom, W.G. Mallard (Eds.), NIST Chemistry WebBook, NIST Standard Reference Database Number 69, National Institute of Standards and Technology, Gaithersburg MD, 20899, 2005.